ORIGINAL ARTICLE

Platinum complexes of curcumin delivered by dual-responsive polymeric nanoparticles improve chemotherapeutic efficacy based on the enhanced anti-metastasis activity and reduce side effects

Yan Chen[a], Chen Chen[a], Xiaojuan Zhang[a], Chuanchuan He[a], Pengxuan Zhao[a], Minsi Li[a], Ting Fan[a], Ruicong Yan[a], Yao Lu[a], Robert J. Lee[b], Muhammad Waseem Khan[a], Muhammad Sarfraz[a], Xiang Ma[a,*], Tan Yang[a,*], Guangya Xiang[a,*]

[a]School of Pharmacy, Tongji Medical College, Huazhong University of Science and Technology, Wuhan 430030, China
[b]College of Pharmacy, the Ohio State University, Columbus, OH 43210, USA

Abstract Platinum-based chemotherapy is used for non-small cell lung cancer (NSCLC). However, it has side effects and minimum efficacy against lung cancer metastasis. In this study, platinum−curcumin complexes were loaded into pH and redox dual-responsive nanoparticles (denoted as Pt−CUR@PSPPN) to facilitate intracellular release and synergistic anti-cancer effects. Pt−CUR@PSPPN was prepared by a nano-precipitation method and had a diameter of ∼100 nm. The nanoparticles showed increased anti-cancer effects both *in vivo* and *in vitro*. In addition, Pt−CUR@PSPPN blocked PI3K/AKT signal transduction pathway and inhibited MMP2 and VEGFR2, resulting in enhanced anti-metastatic activity. Furthermore, reduced side effects were also observed. In conclusion, Pt−CUR@PSPPN provided a novel and attractive therapeutic strategy for NSCLC.

*Corresponding authors. Tel./fax: +86 27 83692793.
    E-mail addresses: xiangma@hust.edu.cn (Xiang Ma), yangtan0120@hust.edu.cn (Tan Yang), gyxiang1968@hotmail.com (Guangya Xiang).

1. Introduction

Lung cancer is the leading cause of cancer mortality worldwide[1,2]. Non-small cell lung cancer (NSCLC) represents the major subtype, accounting for ~80% of this disease[3]. The majority of patients are diagnosed at the intermediate or advanced stages[4], and the five-year survival rate is very low[5]. Chemotherapeutic regimens are still required even if their initial surgeries are curative[6]. However, the invasiveness and metastasis of NSCLC cells present challenges in clinical therapy, leading to treatment failure and ultimately death[7,8]. Therefore, developing novel therapeutic strategies to repress the metastasis of lung cancer cells is of great importance.

Platinum-based chemotherapy followed by a second-line chemotherapeutic agent is the standard treatment for most patients with advanced NSCLC[9,10]. Cisplatin (CDDP) has been extensively applied as a chemotherapeutic agent for the treatment of various cancers including NSCLC. It binds to DNA double helix chains, disturbing DNA replication and inhibiting biosynthesis[11]. However, toxicity to healthy tissues is common, especially in the kidney, caused by the induced reactive oxygen species (ROS), and limited effectiveness against cancer metastasis restricts its clinical application[12,13]. Curcumin (CUR), a natural antioxidant, has been reported to have protective effects on liver and kidney, anti-inflammatory, anti-infection and anti-cancer properties[14−19]. In addition, studies have shown that CUR can decrease the side effects caused by CDDP, especially nephrotoxicity by reducing the ROS level[20]. Moreover, it has been reported that vascular endothelial growth factor receptors (VEGFR) and matrix metalloproteinase 2 (MMP2) can be regulated by CUR to suppress the progress of cancer metastasis[21,22]. Therefore, a combination of CDDP and CUR is a promising approach to enhance the therapeutic window of CDDP, and improve anti-tumor efficacy based on the synergistic effects and enhanced anti-metastasis activity.

Loading small molecule chemotherapy drugs into nanoparticles for delivery, such as polymeric micelles, liposomes or mesoporous silica, allows for increased drug accumulation and better therapeutic effects on tumor based on enhanced permeability and retention (EPR) effect, as well as significantly reduced side effects on normal tissues[23−25]. Whereas, the development of nanoparticles with high entrapping efficiency of CDDP is limited due to its poor solubility[26]. In an early investigation, the platinum complexes of β-diketonate ligands have been developed to improve drug solubility while maintaining its anti-cancer efficacy[27]. Since CUR also contains the structure feature of β-diketonate[28], we synthesized a platinum complex of curcumin, a prodrug in which CUR serves as a leaving group using the similar strategy. In tumor cells, the complexes dissociated into the platinum compound and curcumin, and then provided synergistic efficacy.

Polymeric nanoparticles prepared with biodegradable and biocompatible materials have been used in drug delivery[29]. The nanoparticles not only can enhance the solubility of hydrophobic drugs and improve their stability, but also improve drug efficacy[26]. In addition, the size of polymer nanoparticles is large enough to prevent premature elimination by the glomerular filtration while being small enough to enter cancer tissues through extravasation[30]. In order to avoid the early release of anti-tumor drugs during the circulation *in vivo* and overcome the inability of nanoparticles to effectively release drugs in cancer cells, tumor microenvironment-responsive polymeric nanoparticles have been developed[30]. In previous research, the responsive release of drug-loaded polymeric nanoparticles was mainly achieved by using a single stimulus, such as temperature, pH, reduction, light, and ultrasound[31]. As the research being progressed, more and more complex simulations have been tapped to prepare the stimuli responsive polymeric nanoparticles for rapid drug release at the tumor site[32,33]. Dual-responsive nanoparticles have been developed based on the combination of reduction and pH stimulation[33].

Herein, using disulfide bond and phenylboronate ester as linkages for redox and pH dual-sensitive release, we prepared mPEG−SS−PBAE−PLGA (PSPP) nanoparticles to encapsulate the platinum complexes of curcumin (denoted as Pt−CUR@PSPPN). With the incorporation of an outer polyethylene glycol (PEG) shell, nanoparticles were able to escape the clearance of reticuloendothelial system (RES)[34]. Pt−CUR@PSPPN could maintain stability in blood circulation. However, upon reaching the tumor microenvironment, the linkages could be broken, leading to changes in the physical structure of nanoparticles and then the rapid release of encapsulated drugs. The nanoparticles were evaluated both *in vitro* and *in vivo*, and demonstrated to have improved tolerability and enhanced anti-metastasis activity.

2. Materials and methods

2.1. Materials

CDDP, CUR, methanol-*d* and dimethyl sulfoxide-d_6 were obtained from Sigma−Aldrich Chemical Co. (St. Louis, MO, USA). Dimethylformamide, chloroform, dichloromethane, diethyl ether, pyridine, ethanol, methanol, and sodium carbonate (Na_2CO_3) were purchased from Sinopharm Chemical Reagent Co. (Shanghai, China). Silver nitrate ($AgNO_3$), nitric acid (HNO_3), Triton X-100, 3-(4,5-dimethyl-thiazol-2-yl)-2,5-diphenyl tetrazolium bromide (MTT), Tween-80, mPEG−OH (MW 5000), PLGA-COOH (50/50, 50% lactide and 50% glycolide, MW 15,000), 4-dimethylaminopyridine (DMAP) and 3-aminobenzeneboronic acid (*m*-APBA) were received from Aladdin Reagent Co. (Shanghai, China). Dicyclohexylcarbodiimide (DCC), D,L-dithiothreitol (DTT), *N*-hydroxysuccinimide (NHS), tetramethylammonium hydroxide (TMAOH), 3-hydroxytyramine

hydrochloride (DA) were produced by J&K Chemical Ltd. (Beijing, China). Hoechst 33258 and Sepharose CL-2B columns were acquired from Solarbio Science & Technology Co. Ltd. (Beijing, China). Annexin V-APC/PI Apoptosis Detection Kit was supplied by KeyGEN biotechnology Co. Ltd. (Nanjing, China). $2',7'$-Dichlorodihydrofluorescein diacetate (DCFH-DA), blood urea nitrogen (BUN) and creatinine (CRE) Detection Kit were purchased from Jiancheng Bioengineering Institute (Nanjing, China). Dihydroethidium (DHE) and $4',6$-diamidino-2-phenylindole (DAPI) were obtained from Servicebio Technology Co. Ltd. (Wuhan, China). All reagents and solvents were of analytical or HPLC grade and used without further purification.

Dulbecco's modified Eagle's high glucose medium (DMEM) and fetal bovine serum (FBS) were purchased from Thermo Fisher Scientific (Chicago, IL, USA). A549 and HEK-293 cells were cultured in DMEM supplemented with streptomycin, penicillin and 10% FBS in 5% CO_2 incubators at 37 °C.

BALB/c nude mice (female, 6–8 weeks, 20 ± 2 g) were supplied by Beijing Huafukang Bioscience Technology Co. (Beijing, China). Animal experiments were approved by the Ethics Committee of Huazhong University of Science and Technology (Wuhan, China).

2.2. Synthesis of Pt−CUR complexes

The platinum complexes of curcumin, Pt−CUR, was synthesized as reported earlier[35]. The synthetic procedure was detailed in Supporting Information Scheme S1. First, a mixture of cisplatin (250 mg, 0.83 mmol) and AgNO₃ (270 mg, 1.59 mmol) in 5 mL of dimethylformamide was stirred for 12 h at room temperature in the dark and filtered to remove AgCl. Then, a solution of curcumin (307 mg, 0.83 mmol) and Na_2CO_3 (103 mg, 0.97 mmol) was added dropwise to the filtrate, which was allowed to stir in the dark at room temperature for 5 h under a nitrogen atmosphere. Finally, the solution was filtered and evaporated to approximately 1 mL with the use of a rotary evaporator under vacuum. The product was precipitated in ice-cold diethyl ether, washed with diethyl ether and water, and dried in vacuum. The identity of the product was determined by ^{1}H NMR on a Bruker AV400 (Leipzig, Germany) and ESI-MS on a Bruker Daltonics SolariX 7.0TFT-MS (Leipzig, Germany).

2.3. Synthesis of mPEG−SS−PBAE−PLGA copolymer

2.3.1. Synthesis of mPEG−SS−COOH

Dithiodipropionic anhydride was prepared by the method described previously[36]. mPEG−SS−COOH was synthesized by reacting dithiodipropionic anhydride with mPEG−OH. Briefly, dithiodipropionic anhydride (288 mg, 1.50 mmol), mPEG−OH (5 g, 1.00 mmol) and pyridine (1 mL, 12.40 mmol) were dissolved in 20 mL chloroform. The mixture was refluxed for 6 h at 65 °C, allowed to cool and concentrated to approximately 2 mL by rotary evaporation under vacuum. mPEG−SS−COOH was precipitated by pouring ice-cold diethyl ether into the solution, followed by removal of the diethyl ether, and drying in vacuo.

2.3.2. Synthesis of mPEG−SS−DA

For the synthesis of mPEG−SS−DA, mPEG−SS−COOH (1.05 g, 0.20 mmol), DCC (49.52 mg, 0.24 mmol), NHS (27.62 mg, 0.24 mmol), and DMAP (29.32 mg, 0.24 mmol) were stirred in 20 mL anhydrous dimethylformamide for 4 h under N₂. Then, DA (56.89 mg, 0.30 mmol) was added to the mixture and the reaction mixture was stirred for 48 h at room temperature. At the end of the reaction, the mixture was concentrated and then the crude product was precipitated in ice-cold diethyl ether and dried under vacuum overnight.

2.3.3. Synthesis of PLGA−PBA

PLGA−COOH was grafted with *m*-APBA *via* an acylation reaction. Briefly, PLGA−COOH (1.50 g, 0.10 mmol), DCC (61.90 mg, 0.30 mmol), NHS (34.53 mg, 0.30 mmol), and DMAP (36.65 mg, 0.30 mmol) were added into 25 mL anhydrous dimethylformamide under N₂. The mixture was stirred for 12 h at room temperature. Subsequently, *m*-APBA (41.08 mg, 0.30 mmol) was added to the mixture and stirred for 48 h at room temperature. The mixed solution was then purified by dialysis (MWCO 8 kDa) against ethanol for 24 h to remove unreacted impurities and dimethylformamide. The product was precipitated by pouring the solution into ice-cold methanol and then collected by centrifugation.

2.3.4. Synthesis of mPEG−SS−PBAE−PLGA

The pH and redox dual-sensitive copolymer, PSPP was synthesized by conjugating mPEG−SS−DA to PLGA−PBA. mPEG−SS−DA (1.0 g, 0.19 mmol), PLGA−PBA (1.5 g, 0.10 mmol), and one drop of TMAOH were dissolved in 20 mL anhydrous dichloromethane and refluxed for 24 h under nitrogen stream. After that, dichloromethane was removed and the crude product was hydrated in deionized water to form micelles. The micelles were then purified by dialysis (MWCO 25 kDa) against deionized water for 48 h. The product was finally collected by lyophilization.

The synthesis scheme of PSPP was illustrated in Scheme 1. The pH-sensitive copolymer, mPEG−PBAE−PLGA (PPP) and the redox-sensitive copolymer, mPEG−SS−PLGA (PSP) were synthesized using the same coupling method (Supporting Information Schemes S2 and S3). The copolymers were dissolved in dimethyl sulfoxide-d_6 and characterized by ^{1}H NMR.

2.4. Preparation and characterization of nanoparticles

The pH and redox dual-responsive nanoparticles loaded with Pt−CUR (denoted as Pt−CUR@PSPPN) were prepared as described previously with some modifications[34]. Briefly, 0.5 mg Pt−CUR and 20 mg PSPP copolymer were dissolved in 2 mL dichloromethane/acetone (1:6, *v/v*), which was then added into 10 mL PBS, stirred at 40 °C for 2 h and centrifuged. Subsequently, the suspension was extruded three times through 200 and 100 nm pore-size polycarbonate membrane using a Lipex Extruder from Northern Lipids Inc. (Vancouver, BC, Canada). The residual free drug was removed by size exclusion chromatography on Sepharose CL-2B columns. Pt−CUR@PPPN and Pt−CUR@PSPN were also prepared using the same method.

The average zeta potential and particle size of Pt−CUR@PSPPN were determined on a Zeta PALS Zeta Potential Analyzer from Brookhaven Instruments Corporation (Austin, TX, USA). A JEOL 100CX II transmission electron microscope (Tokyo, Japan) was used to observe and photograph the morphology.

The encapsulation efficiency of drugs was measured by dissolving nanoparticles in HNO₃ and quantifying Pt−CUR
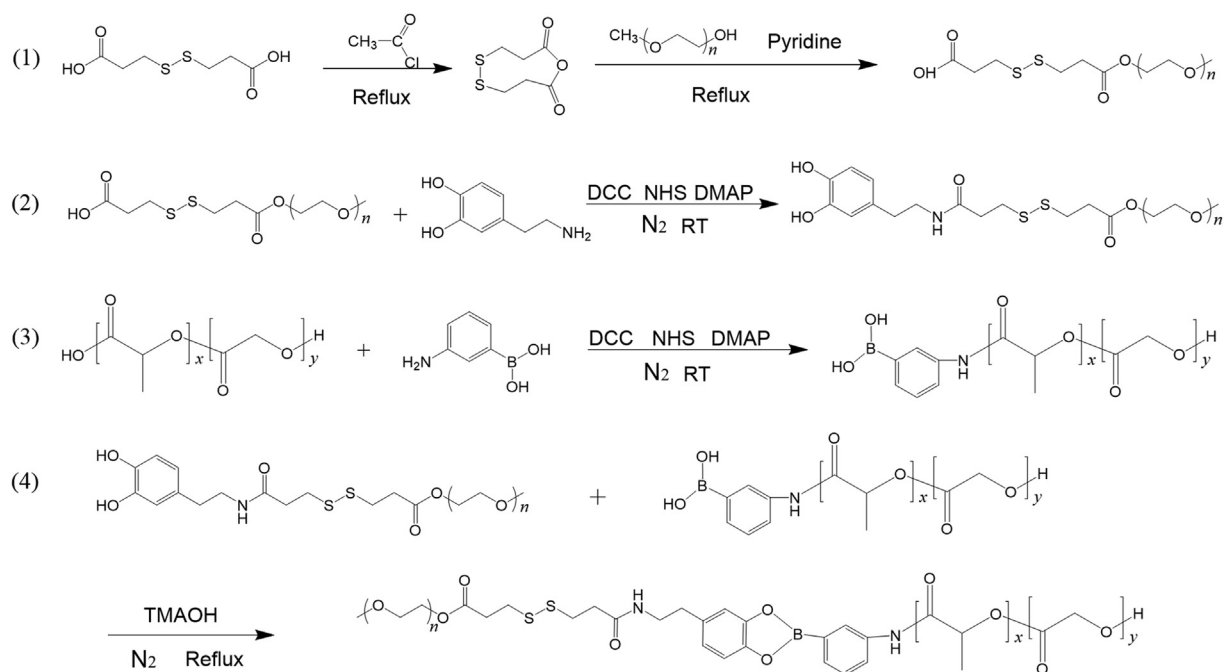
Scheme 1   Synthesis scheme of mPEG−SS−PBAE−PLGA.

concentration by SpectrAA-24OFS atomic absorption spectrometer (Varian, Palo Alto, CA, USA).

2.5. Cytotoxicity assay

MTT assay was performed to investigate the cytotoxicity of empty nanoparticles. A549 cells were seeded in 96-well plates at a density of 1×10^4 cells per well and allowed to attach overnight. Cells were then incubated with 100 μL culture media containing serial dilutions of PPPN, PSPN, and PSPPN. The plates were subsequently incubated for 24 or 48 h. The cell viability was then calculated.

2.6. In vitro stability

Stability of Pt−CUR@PSPPN after storage at 4 °C for 4 weeks was evaluated. Samples were withdrawn weekly and measured in triplicate at room temperature. The zeta potential and particle size were evaluated using the method as described above.

2.7. In vitro drug release

The release profile of Pt−CUR@PSPPN was studied by dynamic dialysis method. Pt−CUR@PSPPN (1.5 mL, 2.25 mg Pt−CUR) was placed into prepared dialysis bags (MWCO 10 kDa) and dialyzed against 400 mL PBS solutions containing 0.5% Tween-80 and 25% (v/v) ethanol at 37 °C under mild stirring (120 rpm, IKA C-MAG HS7 magnetic stirrer, Schwarzwald, Germany). For dual sensitivity, nanoparticles were incubated with or without 10 mmol/L DTT at pH 7.4 or 5.5. Pt−CUR@PPPN and Pt−CUR@PSPN were kept at pH 5.5 with 10 mmol/L DTT as a control. At selected time intervals from 0 to 72 h, an aliquot (50 μL) was taken from the dialysis bag and replaced with an equal volume of fresh medium. The concentrations of Pt−CUR in the samples were determined as described above.

2.8. In vitro cellular uptake

2.8.1. Fluorescence microscopy
A549 cells were seeded in 6-well plates at a density of 2×10^5 cells per well and incubated overnight at 37 °C. Free Pt−CUR or Pt−CUR@PSPPN (10 μmol/L Pt−CUR per well) were then added to the media and incubated with cells for 4 h. PBS was used as control. After incubation, the cells were washed with cold PBS 3 times, fixed with 4% paraformaldehyde for 15 min and captured on an Olympus SZX12 fluorescence microscope (Tokyo, Japan).

2.8.2. FACS analysis
A549 cells (2×10^5 cells per well) were plated in 6-well plates, incubated overnight, and treated with free Pt−CUR or Pt−CUR@PSPPN (10 μmol/L Pt−CUR per well) followed by incubation at 37 °C at 1, 4 and 8 h. For measurement of uptake, cells were washed with cold PBS 3 times and then trypsinized, redispersed and enumerated by a Becton Dickinson LSRIIflow cytometer (San Jose, CA, USA).

2.9. Platinum−DNA adduct staining

In order to form the platinum−DNA adduct at the tumor site, the leaving group, CUR was dissociated from Pt−CUR firstly. The specific dissociation of the Pt and CUR was investigated using F-4600 fluorescence spectrophotometer (Hitachi, Tokyo, Japan) with the excitation/emission wavelength at 430/530 nm. Briefly, 5 mg Pt−CUR was dissolved in 30 mL methanol/water (1:1, v/v) with the presence or absence of 10 mmol/L glutathione (GSH). An equimolar amount of curcumin (2.80 mg) was used as control. The solutions were incubated in the dark under nitrogen stream. At 10, 30 min, 1, 2, 4, 8 and 12 h, an aliquot (2 mL) was taken from the solution and the fluorescence intensity was measured.

The platinum−DNA adducts were examined using flow cytometry by anti-cisplatin-modified DNA antibody [CP9/19]

(Abcam, Cambridge, UK). Cells in culture were treated with free CDDP, free CUR, a combo of free drugs, free Pt−CUR, Pt−CUR@PPPN, Pt−CUR@PSPN, or Pt−CUR@PSPPN, with untreated cells as control. After 24 h incubation, the cells were dispersed in cold PBS, fixed with 4% PFA for 15 min and permeated with 0.1% Triton X-100. The cells were then incubated with the primary antibody (1:200) at 4 °C overnight. Cy3-labeled goat anti-Rat IgG H&L antibody (1:200, Abcam) was used as the secondary antibody.

2.10. Cell cytotoxicity and apoptosis study

MTT assay was conducted to detect *in vitro* viability of free CDDP, free CUR, a combo of free drugs, free Pt−CUR, as well as Pt−CUR@PPPN, Pt−CUR@PSPN, and Pt−CUR@PSPPN. Briefly, A549 cells were seeded in 96-well plates at a density of 1×10^4 cells per well and incubated overnight at 37 °C. Cells were then incubated with serial dilutions of drug formulations for 24 h. The portions of viable cells were measured using MTT according to the user's manual. Combination index (CI) analysis of CDDP/CUR at molar ratio 1:1 was analyzed by Chou-Talalay method[37]. The occurrence of synergistic effect was determined by plotting the CI *versus* the fraction of cells affected (Fa). CI values between Fa 0.2 to 0.8 are therapeutically relevant and CI values less than 1 or more than 1 indicate synergism or antagonism of drug combinations, respectively. Moreover, half-maximal inhibitory concentration (IC_{50}) was used to evaluate the cytotoxic effects of drugs.

The qualitative apoptosis of A549 cells treated with different drug formulations was determined using Hoechst 33258 staining method. A549 cells were plated in 6-well plates at a density of 2×10^5 cells per well. After 24 h incubation, cells were treated with drugs (20 μmol/L Pt or CUR) for an additional 24 h. Then, the cells were washed 3 times with cold PBS, stained with Hoechst 33258 (10 μg/mL) for 10 min at 37 °C in the dark and visualized on a fluorescence microscope.

To detect quantitative apoptosis, allophycocyanin-conjugated annexin V /propidium iodide (Annexin V-APC/PI) double staining was performed. A549 cells were seeded in 12-well plates, followed by overnight incubation. The cells were then treated with different drug formulations, with untreated cells as control. After 24 h of incubation at 37 °C, the cells were washed with cold PBS 3 times, trypsinized, centrifuged, and resuspended in annexin V binding buffer. Annexin V-APC and PI (5 μL each) were then added and incubated with cells for 15 min in the dark. Finally, the cell samples were analyzed using a flow cytometer.

2.11. Transwell migration and invasion assay

Transwell insert chambers with 8 μm pore size and 6.5 mm in diameter (Corning, San Diego, CA, USA) were used for migration and invasion assay. Briefly, for the migration assay, 5×10^4 A549 cells were placed in the inner chambers, and were exposed to serum-free medium containing PBS or different drug formulations (20 μmol/L Pt or CUR). Medium containing 10% serum was added to the lower chambers to stimulate cell migration. Following incubation for 24 h, non-migrated cells on the upper surface of the polycarbonate filter were gently removed by a cotton swab. Migratory cells on the lower compartment were fixed with 4% paraformaldehyde for 5 min, stained with 1% crystal violet solution and then observed on an Olympus microscope. Three random fields of view from different chambers were

counted for each treatment. The cell invasion activity was also assessed using transwells. A minor modification was that the transwell polycarbonate membrane inserts were pre-coated with Matrigel (Sigma−Aldrich). The remaining experimental procedures were the same as above in the migration assay.

2.12. Wound healing assay

Migratory ability of cells was assessed by a wound healing assay. A549 cells in exponential phase were seeded in 6-well plates at a density of 5×10^5 cells per well and allowed to reach 100% confluence overnight. Cell monolayers were wounded with a 200 μL pipette tip and washed with the medium in a sterile environment. Subsequently, the cells were exposed to serum-free medium containing PBS or different drug formulations (20 μmol/L Pt or CUR). Images were taken at 0 and 24 h using an Olympus microscope. Then migration distance was measured.

2.13. Western blot

A549 cells were seeded in 6-well plates and treated with different drug formulations (20 μmol/L Pt or CUR) for 24 h. Proteins were extracted by RIPA lysis buffer containing 2% cocktail, 1% protease inhibitor and 1% PMSF. Proteins were then separated on a 10% SDS-PAGE gel and transferred to PVDF membranes. The membranes were blocked with 5% skim milk dissolved by TBS−0.1% Tween 20 (TBST) for 1 h and incubated with monoclonal antibodies against β-tubulin (1:1000, Cell Signaling, Danvers, MA, USA), VEGFR2 (1:1000, Abcam), p-VEGFR2 (1:1000, Cell Signaling), MMP2 (1:1000, Cell Signaling), AKT (1:1000, Cell Signaling), p-AKT (1:1000, Cell Signaling), BCL-2 (1:1000, Cell Signaling), NF-κB (1:1000, Cell Signaling), cleaved-caspase3 (1:1000, Cell Signaling), and BAX (1:1000, Cell Signaling) overnight at 4 °C. The membranes were then washed 3 times with TBST, incubated with a secondary antibody (1:2000, Cell Signaling) for 1 h at room temperature and washed three times with TBST again. The target proteins were conjugated with an ECL kit and detected by GeneGenome5 chemiluminescence system (Syngene, Cambridge, UK).

2.14. Kidney cell protection in vitro

Intracellular ROS level was detected to investigate the kidney cell protection of nanoparticles *in vitro*. HEK-293 cells cultured on 6-well plates at a density of 5×10^5 cells per well were incubated overnight and treated with medium containing different drug formulations (10 μmol/L Pt or CUR) for 24 h. PBS was used as control. Cells were then incubated with DCFH-DA (10 μmol/L) for 30 min at 37 °C, trypsinized and resuspended. After that, the fluorescence of HEK-293 cells was detected by flow cytometer.

2.15. Biodistribution study

A549 cells were subcutaneously injected in the right front flank of female BALB/c nude mice to initiate a xenograft mouse model. For biodistribution study, the mice were randomly divided into two groups ($n = 5$) and given free Pt−CUR or Pt−CUR@PSPPN with the Pt−CUR dose of 1 mg/kg by tail intravenous injection. At time intervals of 1, 6, 12 and 24 h after injection, tissue samples were collected after sacrificed. The samples were then rinsed by saline, weighed, freeze-dried and digested by HNO_3. Pt−CUR

concentration in the samples was determined by atomic absorption spectrometer as described above.

2.16. Anti-tumor efficacy study in vivo

Therapeutic effect *in vivo* was investigated in A549 xenograft tumor-bearing nude mice. When tumor volume reached around 100 mm³, mice were randomly distributed into eight groups (5 mice for each) and given tail vein injection of different drug formulations including free CDDP, free CUR, combo of free drugs, free Pt−CUR, as well as Pt−CUR@PPPN, Pt−CUR@PSPN, and Pt−CUR@PSPPN (2 mg/kg of CDDP, 2.45 mg/kg CUR or 4.39 mg/kg Pt−CUR) every 3 days for a total of 4 doses. Tumor volume and body weight were recorded every 2 or 3 days. During the sacrifice, blood was collected *via* the retro-orbital and the serum was isolated for the measurement of biochemical indexes of the kidney, including BUN and CRE. Tumors were collected, weighed and processed for hematoxylin and eosin (H&E) staining and immunohistochemical analysis including CD31 (Cell Signaling), VEGF (Cell Signaling), and MMP2. To detect the ROS level, frozen sections of kidneys were incubated with ROS fluorescent probe-DHE for 30 min in the dark at 37 °C. The sections were then washed three times with PBS, stained with DAPI for 10 min at room temperature and captured on a fluorescence microscope. ROS in the kidneys was colored by red fluorescence.

2.17. Metastasis inhibition

To establish the metastasis model, female BALB/c nude mice were given tail vein injection of A549 cells suspension (10⁶ cells in 0.15 mL saline). The mice were randomly divided into six groups (n = 5) and treated with PBS, free

CDDP, free CUR, combo of free drugs, free Pt−CUR and Pt−CUR@PSPPN (2 mg/kg of CDDP, 2.45 mg/kg CUR or 4.39 mg/kg Pt−CUR) on days 2, 4, 6 and 8. Three weeks later, mice were euthanized. The lungs were excised, fixed with Bouin's solution and photographed. The metastatic lung nodules were observed and counted under magnifying glass.

2.18. Statistical analysis

Quantitative results were presented as mean ± standard deviation (SD). Statistical significance was assessed by Student's *t*-test or one-way analyses of variance (ANOVA) with Dunnett's post-test (SPSS Software, Chicago, IL, USA). A value of $P < 0.05$ was considered significant and $P < 0.01$ was considered highly significant.

3. Results

3.1. Synthesis of Pt−CUR and PSPP copolymer

Pt−CUR complexes were successfully synthesized as detailed in Scheme S1 and characterized by ¹H NMR in methanol-d and ESI-MS in methanol. As shown in Supporting Information Fig. S1, ¹H NMR peaks assigned for Pt−CUR are: δ 7.64 (d, 2H), 7.20 (d, 2H), 7.11 (m, 2H), 6.80 (d, 2H), 6.55 (d, 2H), 5.87 (s, 1H), 3.90 (s, 6H) ppm. ESI-MS (Supporting Information Fig. S2), $C_{21}H_{25}N_3O_9Pt$: $[M-NO_3]^+$, Calcd. for 596.1360, Found 596.1359.

The synthesis scheme of mPEG−SS−PBAE−PLGA is illustrated in Scheme 1. PSPP copolymer was synthesized *via* a four-step procedure. The successful synthesis of copolymers was confirmed by ¹H NMR analysis in dimethyl sulfoxide-d_6 (Fig. 1 and Supporting Information Fig. S3). As shown in Fig. 1, the
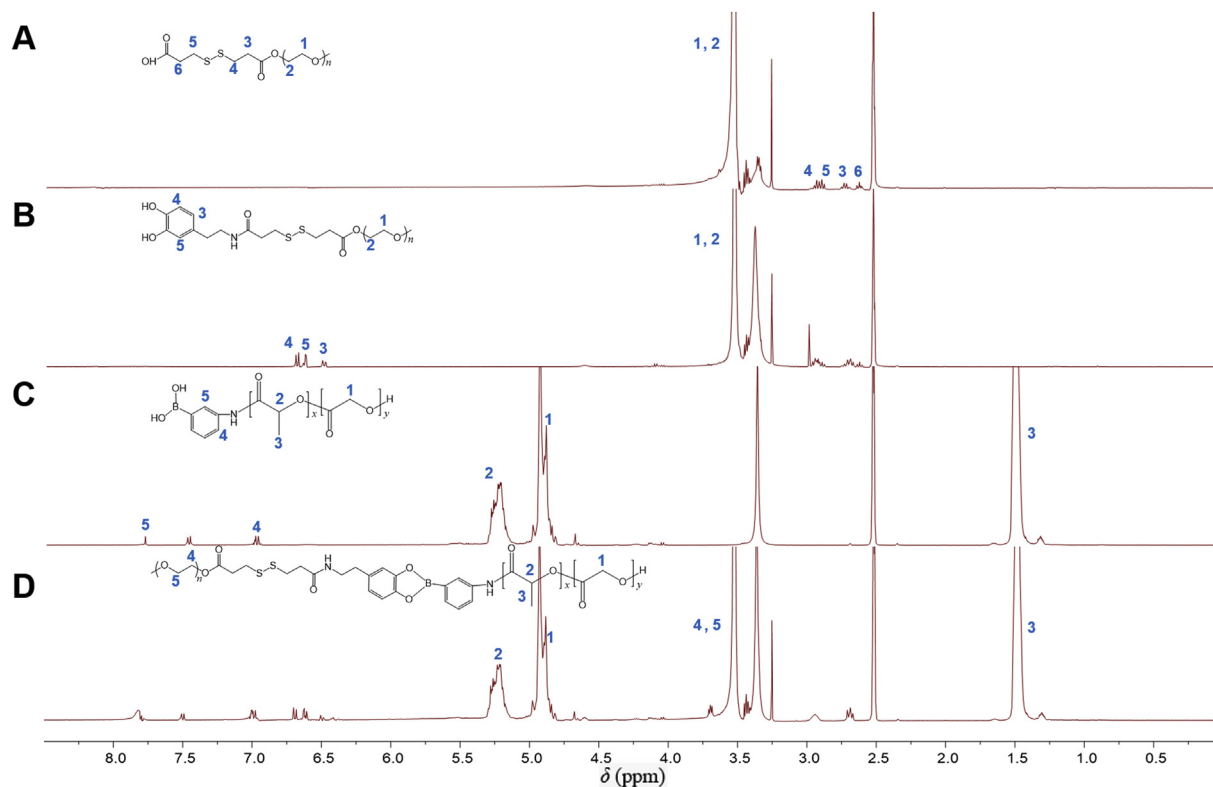
Figure 1 ¹H NMR spectra of polymer derivatives. mPEG−SS−COOH (A), mPEG−SS−DA (B), PLGA−PBA (C), and mPEG−SS−PBAE−PLGA (D) in dimethyl sulfoxide-d_6. Characteristic peaks as marked in the graphs.

results show principal peaks (in ppm) assigned to the mPEG moiety (δ 3.62 ppm), the PLGA moiety (δ 1.49, 4.93 and 5.23 ppm), the disulfide bond moiety (δ 2.62, 2.72, 2.89 and 2.92 ppm), and the phenylboronate ester moiety (δ 6.47−6.71 and 7.01−7.85 ppm).

3.2. Preparation and characterization of nanoparticles

The nano-precipitation method was employed for the preparation of nanoparticles, similarly to previous reports[34]. The synthesis route of Pt−CUR@PSPPN is illustrated in Fig. 2A. As the solvent evaporated, the nanoparticles were easily self-assembled in PBS. The size of nanoparticles was uniform upon the extrusion through polycarbonate membrane using a Lipex Extruder. Residual-free Pt−CUR was then removed by size exclusion chromatography on a Sepharose CL-2B column. The design of Pt−CUR@PSPPN is shown in Fig. 2B. The average particle diameters of Pt−CUR@PSPPN were 154.87 ± 10.32 nm by dynamic light scattering (DLS) measurement (Fig. 2D). Surface morphology of nanoparticles was observed and photographed by transmission electron microscope (TEM, Fig. 2C). The particle size obtained by TEM was slightly smaller than the values measured by the DLS method. The zeta potential and polydispersity index were −20.8 ± 3.6 and 0.115 ± 0.012 mV, respectively (Fig. 2D), indicating a good dispersion. Drug encapsulation efficiency was 90.3 ± 3.1% (Fig. 2D).

As shown in Supporting Information Table S1, other nanoparticles have similar physicochemical properties compared with Pt−CUR@PSPPN.

3.3. In vitro properties

To investigate the biocompatibility of nanoparticles, the MTT assay was performed. Blank nanoparticles including PPPN, PSPN, and PSPPN were prepared using the same method as described above. The results of the MTT assay are shown in Fig. 3A and B. After incubation for 24 h, almost no cell death in A549 cells was observed. When the incubation time reached 48 h, cells treated with serial dilutions still had a survival rate of about 90%, which indicated the good biocompatibility and safety of blank nanoparticles.

Stability of Pt−CUR@PSPPN after storage at 4 °C for 4 weeks was analyzed by observing the changes in particle size and zeta potential. As shown in Fig. 3C, the average particle size at the start and end points are 154.86 and 163.81 nm, respectively. The zeta potential of nanoparticle was −20.80 mV on the first day and −21.73 mV after storage at 4 °C for one month. No significant variation in particle size and zeta potential was detected, which indicated the excellent stability of Pt−CUR@PSPPN during storage.

The pH and redox-dependent release profile were studied by dynamic dialysis method at pH 7.4 or 5.5 in the presence or absence of 10 mmol/L DTT. pH 7.4 was used to simulate the acid value of blood while pH 5.5 and 10 mmol/L DTT corresponded to the physiological environment in the endosomes of cancer cells, respectively. As expected, Pt−CUR@PSPPN exhibited redox- and pH-sensitive release (Fig. 3D). In addition, compared to the excellent stability during storage, more drugs were released from nanoparticles during dynamic dialysis at 37 °C. It may be contributed to the temperature. According to the literature, inter-micelle chain movement and critical micelle concentration (CMC) of polymer nanoparticle increased at greater temperature, demonstrating the influence of temperature on thermodynamic stability[38]. Therefore, as the temperature raised, more drugs were released from nanoparticles[39]. In pH 7.4 PBS solution, without DTT, about 20% encapsulated drug was released from the nanoparticles at 24 h and less than 40% was released within 72 h. However, an initial burst release took place at pH 5.5 or in the

Sample	Particle size (nm)	Zeta potential (mV)	PDI	Encapsulation efficiency (%)
Pt−CUR@PSPPN	154.87±10.32	−20.8±3.6	0.115±0.012	90.3±3.1
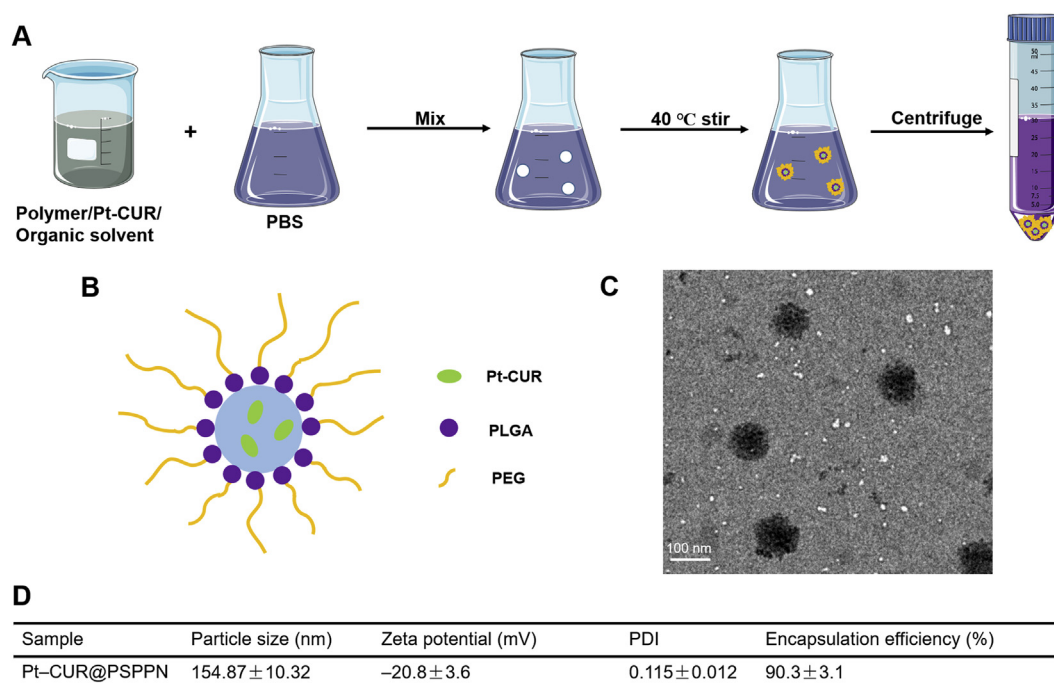
Figure 2 Synthesis scheme and characteristics of nanoparticles. (A) Schematic of nanoparticle synthesis, (B) nanoparticle structure, (C) TEM image of Pt−CUR@PSPPN and (D) physicochemical properties of nanoparticles. Data are expressed as mean ± SD ($n = 3$).
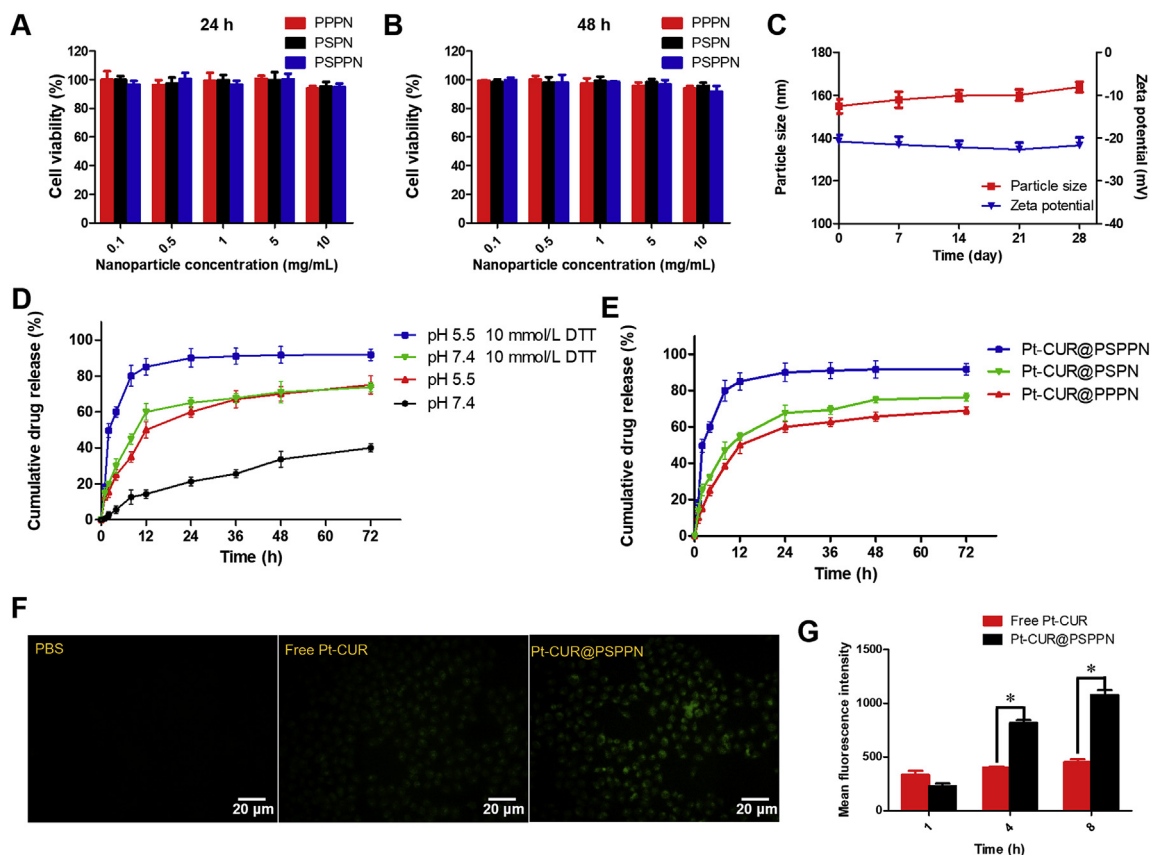
Figure 3 *In vitro* properties of nanoparticles. Viabilities of A549 cells treated with PPPN, PSPN, and PSPPN for 24 (A) or 48 h (B). (C) Stability of nanoparticles during storage as measured by the particle size and zeta potential for 4 weeks. (D) *In vitro* release of Pt−CUR from Pt−CUR@PSPPN incubated with or without 10 mmol/L DTT at pH 7.4 or 5.5. (E) *In vitro* drug release profiles of Pt−CUR@PPPN, Pt−CUR@PSPN and Pt−CUR@PSPPN kept at pH 5.5 with 10 mmol/L DTT. The uptake of free Pt−CUR and Pt−CUR@PSPPN by A549 cells. (F) Fluorescence microscope images of cells incubated for 4 h. PBS was used as a control. (G) Mean fluorescence intensity in cells at 1, 4 and 8 h after incubation. Data are expressed as mean $\pm$ SD ($n = 3$). $^{*}P < 0.05$, $^{**}P < 0.01$.

presence of 10 mmol/L DTT, and more than 50% of incorporated Pt−CUR was released within 12 h. In the following 60 h of incubation, the cumulative release percentages reached about 70%. Moreover, when exposed to the acidic and reductive environment, the drug released more quickly, where 60% of the entrapped drug was released at 4 h, and more than 90% was released at 72 h. Pt−CUR@PPPN and Pt−CUR@PSPN kept at pH 5.5 with 10 mmol/L DTT were used as controls. As shown in Fig. 3E, the encapsulated drug release percentages of Pt−CUR@PSPN and Pt−CUR@PSPN are 76% and 72%, respectively, which are below that of Pt−CUR@PSPPN (90%).

3.4. *In vitro* cellular uptake

Fluorescence microscopy and FACS analysis were performed to investigate the cellular uptake of Pt−CUR@PSPPN and free Pt−CUR in A549 cells based on the intrinsic green fluorescence of drugs. As shown in Fig. 3F, free Pt−CUR can enter into cells after 4 h incubation *in vitro*. Stronger green fluorescence was observed when the cells were incubated with Pt−CUR@PSPPN. In order to further quantify the uptake, the intracellular drug concentration was measured by flow cytometer at the time points of 1, 4 and 8 h. FACS analysis indicated that intracellular fluorescence intensity of free Pt−CUR treated cells were low at 1, 4

and 8 h (Fig. 3G). However, the intracellular uptake of nanoparticles exhibited a time dependence, and was much higher than that of cells treated with the free drug at 4 and 8 h, which was consistent with the result of fluorescence microscopy.

3.5. Cell cytotoxicity and apoptosis study

It has been reported that the fluorescence intensity of free curcumin is dampened upon complexation with platinum and the increase of emission intensity indicates the release of curcumin[35]. Therefore, the specific dissociation of the Pt and CUR was studied by the change of fluorescence. According to the literature, Pt−CUR complex could release Pt and CUR in the presence of GSH[40]. Our result was consistent with this. As shown in Supporting Information Fig. S4, almost all CUR is dissociated from complex in 10 mmol/L GSH within 4 h. However, no obvious change of fluorescence intensity was observed even at 12 h without GSH. The Pt−DNA adducts were examined to further prove that platinum could dissociate from complexes and crosslink to DNA chain by the usage of CP9/19, an antibody enables the quantification of cisplatin-induced adducts on DNA. Fig. 4A and B showed the mean fluorescence intensity (MFI) of A549 cells treated with different drug formulations, which represented the amount of Pt−DNA adducts. Free Pt−CUR induced a

similar accumulation of modified DNA as free CDDP and combo of free drugs did. MFI of treated cells was enhanced after loading the drug into the nanoparticles and Pt−CUR@PSPPN led to the strongest fluorescence.

To evaluate the *in vitro* cytotoxicity of different drug formulations, MTT assay was employed on A549 cells. *In vitro* synergy study using Chou-Talalay method indicated that combination of CDDP and CUR exhibited synergism at molar ratio 1:1 (Supporting Information Fig. S5). As illustrated in Fig. 4C, all drugs show inhibitory effects on the tumor cells. The IC$_{50}$ of free CDDP and free CUR are 16.06 and 36.49 μmol/L, respectively. When combining the two free drugs, the IC$_{50}$ is reduced to 12.07 μmol/L. A significant reduction in IC$_{50}$ was observed after loading Pt−CUR into the nanoparticles. Pt−CUR@PSPPN

group exhibited 4 times stronger cell inhibition than the free drug.

We further stained A549 cells with Hoechst 33258 and then examined and photographed the nuclear morphology *via* fluorescence microscopy (Fig. 4D). Bright staining and condensed nuclei were observed to be increased in Pt−CUR@PSPPN treated cells, suggesting more apoptosis.

To detect quantitative apoptosis of A549 cells, annexin V-APC/PI double staining was conducted. As shown in Fig. 4E, free CUR does not induce much apoptosis while free CDDP, free drug combination and free Pt−CUR treatments slightly accelerated A549 cell apoptosis. All formulations of nanoparticles showed increased cytotoxicity compared to those with free drugs. The highest percentage in the early and late apoptotic cells was
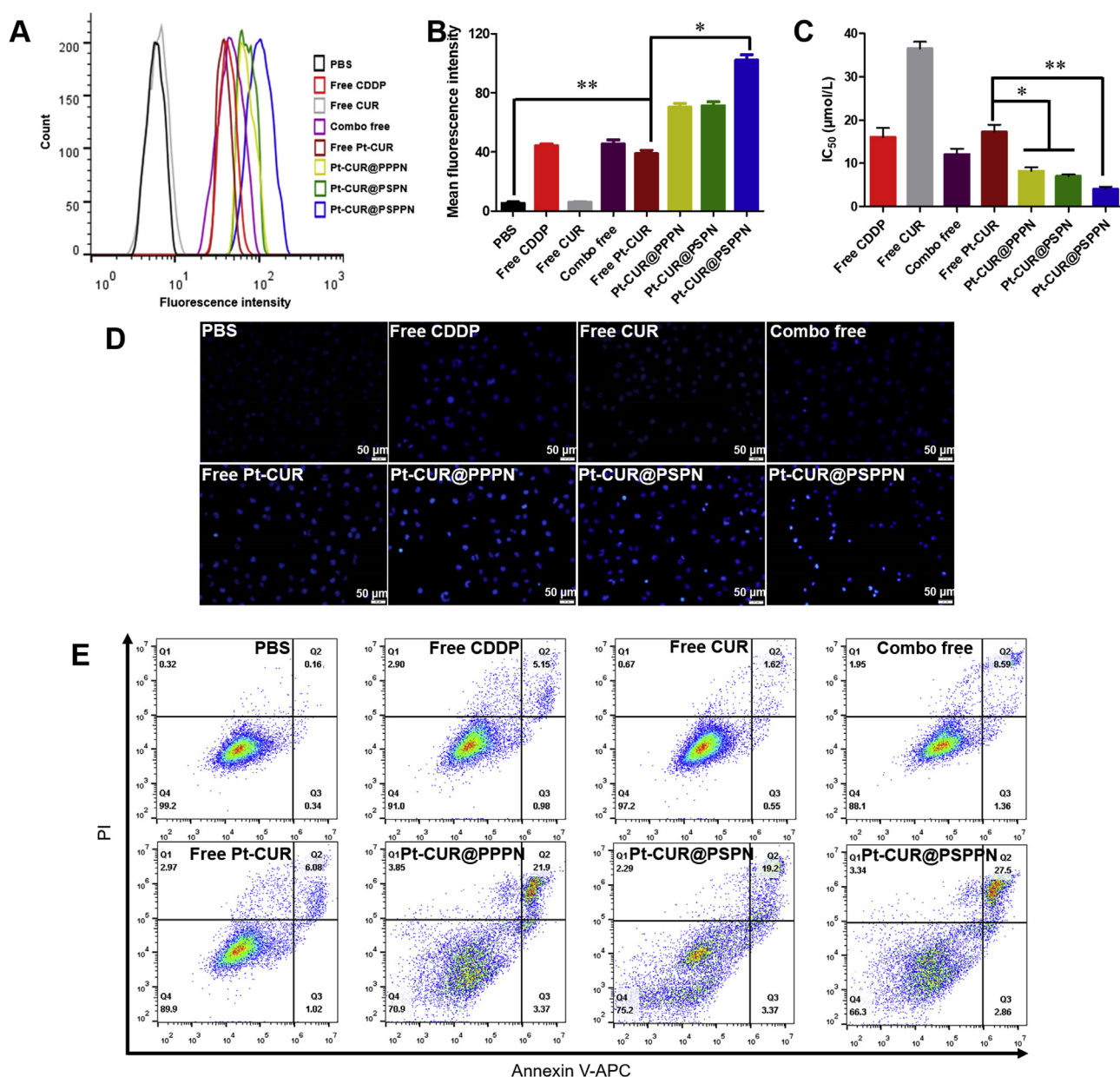
Figure 4 Anti-tumor effects in A549 cells. (A) Platinum−DNA adducts were examined using flow cytometry by CP9/19 antibody. (B) The quantification of Platinum−DNA adducts. (C) Viabilities of A549 cells treated with various drug formulations for 24 h. IC$_{50}$ was calculated. (D) Hoechst 33258 nucleus staining. (E) Annexin V-APC/PI double staining cell apoptosis. Untreated cells were used as control. Data are expressed as mean ± SD ($n = 3$). $^*P < 0.05$, $^{**}P < 0.01$.

detected in Pt−CUR@PSPPN treatment group, which was consistent with the result of MTT. All these data indicate that Pt−CUR@PSPPN could exert expected higher inhibition of tumor cell growth *in vitro*.

3.6. Synergetic anti-metastasis effect of nanoparticles

Migration, invasion and wound healing assays were used to investigate the synergetic anti-metastasis effect of nanoparticles. As observed in Fig. 5A−D, free CUR, free CDDP, combo free, and free Pt−CUR significantly suppress migration and invasion of A549 cells. Although all nanoparticles resulted in a greater inhibitory effect than free drug treatment, Pt−CUR@PSPPN presented much stronger inhibition than other nanoparticles. Likewise, wound healing assay showed that both CDDP and CUR blocked cell motility (Fig. 6A and B). Meanwhile, Pt−CUR significantly suppressed the migration of A549 cells. A stronger inhibition on wound healing was presented in A549 cells treated with Pt−CUR@PSPPN, compared with other treatments.

In order to establish the anti-metastasis and anti-tumor mechanisms of Pt−CUR@PSPPN, the expression of metastasis-related and apoptosis-related proteins was measured (Fig. 6C and D). β-Tubulin was used as a loading control. Expression of p-AKT after treatment with either free drugs or nanoparticles was significantly down-regulated. Pro-apoptotic proteins BAX and cleaved caspase-3 were up-regulated. Meanwhile, anti-apoptosis genes BCL-2 and NF-κB, and metastasis-related factors MMP2 and p-VEGFR2 were down-regulated. The down-regulation was consistent with the results of transwell and wound healing assays.

3.7. Kidney cell protection in vitro

The increased ROS level is a major reason of cisplatin nephrotoxicity. Thus, intracellular ROS level of HEK-293 cells was examined to investigate the kidney cell protection *in vitro*. As shown in Supporting Information Fig. S6, the fluorescence intensity is slightly increased after exposure to free CDDP compared to the control group. However, no significant difference was observed between PBS and treatment containing CUR. It may be attributed to the antioxidant activity of CUR. All these data indicated that CUR can protect the kidney cell treated with CDDP *in vitro* by reducing the ROS level.

3.8. Biodistribution

The biodistribution study was performed by giving a single injection of free Pt−CUR or Pt−CUR@PSPPN to A549 xenograft tumor-bearing nude mice through the tail vein. The concentrations of Pt−CUR in major organs at different times post-injection are shown in Fig. 7A. For mice treated with free Pt−CUR, the drug was mainly detected in the liver and the kidney, and the concentration increased with time in the kidney which indicated rapid elimination. At 1, 6, 12 and 24 h after injection, concentrations of drugs in tumor site delivered by nanoparticles were 1.45, 3.31, 2.61 and 0.93 μg/g, respectively. However, the concentrations in the free drug group were only 1.42, 1.25, 0.67 and 0.58 μg/g, respectively. Pt−CUR@PSPPN showed higher accumulation in tumor compared with free Pt−CUR.

3.9. In vivo antitumor activity and toxicity

Antitumor activity and toxicity *in vivo* were investigated in A549 xenograft tumor-bearing nude mice. Mice were given tail vein injection of different drug formulations including free CDDP, free CUR, a combo of free drugs, free Pt−CUR as well as Pt−CUR@PPPN, Pt−CUR@PSPN and Pt−CUR@PSPPN every 3 days on day 9, 12, 15 and 18 after tumor inoculation. Tumor volume was recorded to evaluate anti-tumor efficiency. As shown in Fig. 7B,
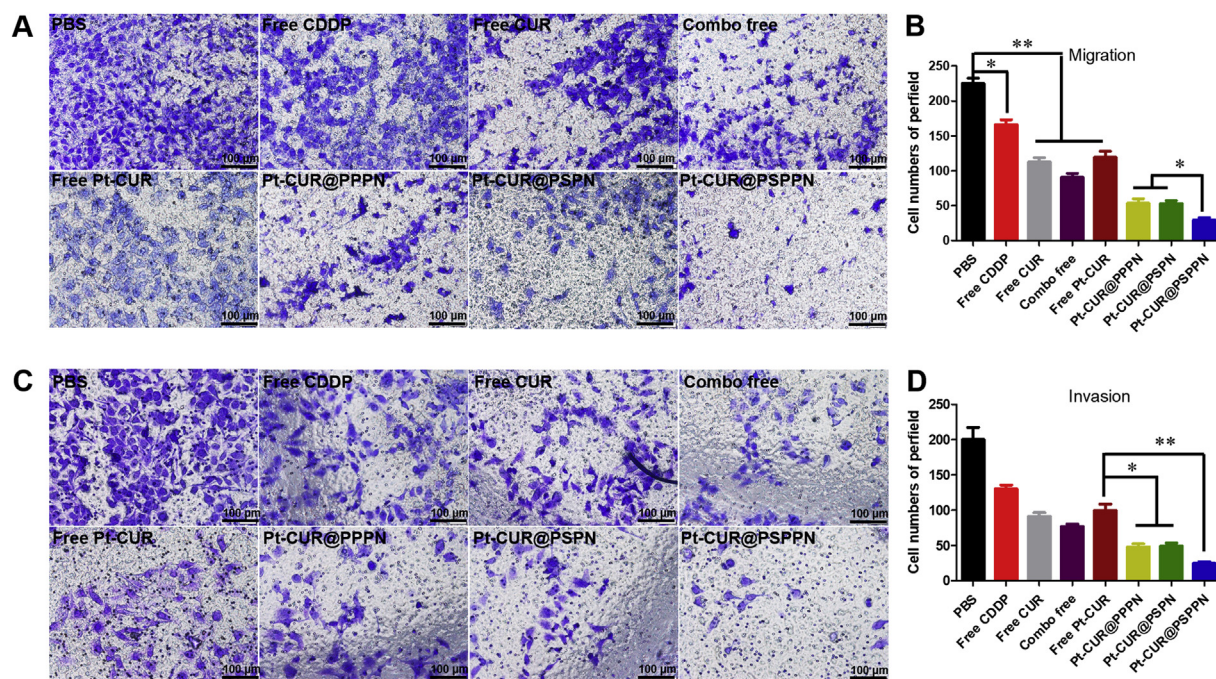
Figure 5 Activities against migration and invasion for the nanoparticles. Migration (A) and invasion (C) activities of A549 cells treated with free CDDP, free CUR, combo free, free Pt−CUR as well as Pt−CUR@PPPN, Pt−CUR@PSPN and Pt−CUR@PSPPN. The quantification of migration (B) and invasion (D) activities. Data are expressed as mean $\pm$ SD ($n = 3$). $^{*}P < 0.05$, $^{**}P < 0.01$.
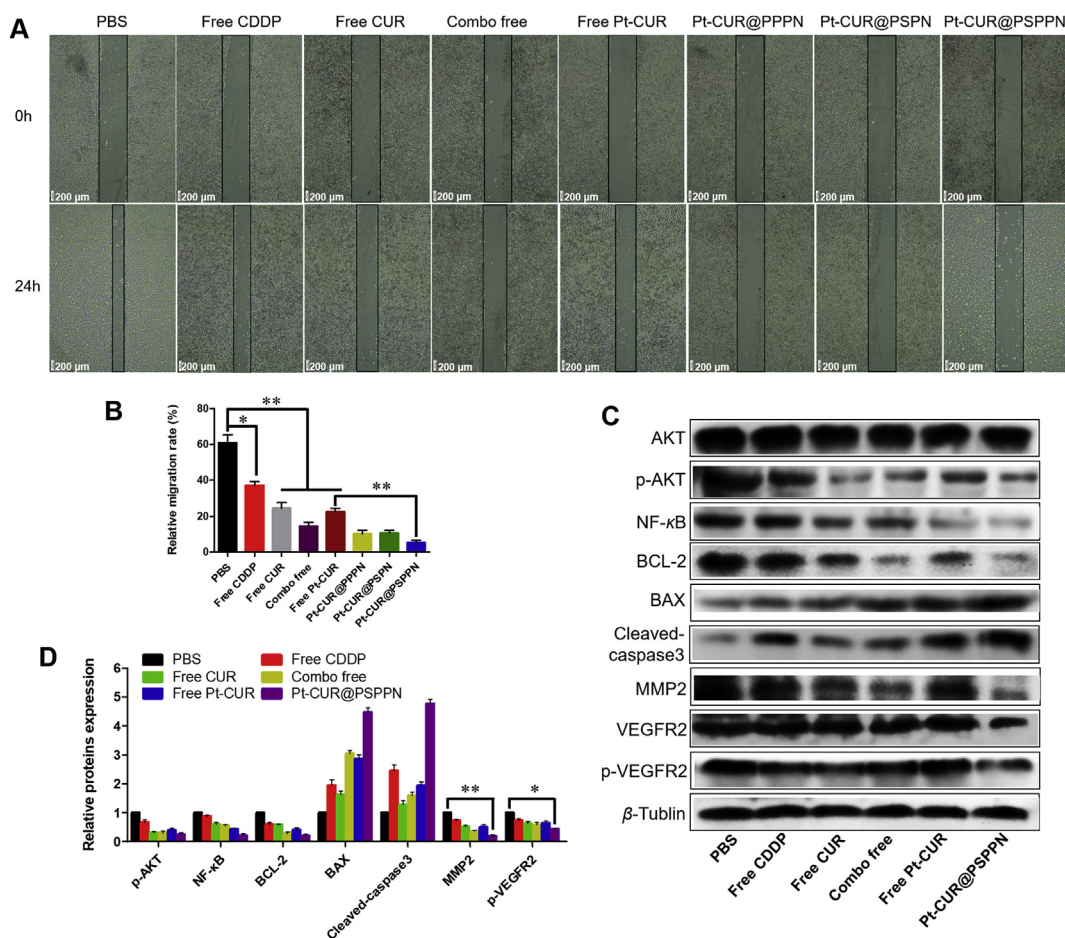
Figure 6 Synergetic anti-metastasis effect of nanoparticles. (A) Images of wound healing assay at 0 and 24 h. (B) The quantification of wound healing assay was calculated as: percent closure (%) = length of cell migration/width of wounds × 100. Percent closure of control group was standardized as 100%. (C) Western blotting of indicated proteins expression in A549 cells treated with free CDDP, free CUR, combo free, free Pt−CUR and Pt−CUR@PSPPN. (D) The relative proteins expression was calculated by the signal intensity of protein bands. Data are expressed as mean ± SD (n = 3). $^{*}P < 0.05$, $^{**}P < 0.01$.

tumors treated with PBS or free CUR proliferate faster than in other groups. Free CDDP, combo free, and free Pt−CUR were all effective, with the final mean tumor volumes of 651.79, 545.14 and 501.89 mm^3, respectively. Notably, a better inhibition against the tumor growth was observed with the consecutive treatment of nanoparticles and Pt−CUR@PSPPN exhibited optimal therapeutic effect *in vivo*, which was consistent with our expectations. At the end of the experiment, tumors were collected, photographed and weighed (Fig. 7C and D). These results were in accordance with the conclusion of the growth curve as described above.

Body weight change was considered an important indicator of general systemic toxicity. As shown in Fig. 8A, almost all drug formulations are well tolerated while free CDDP induced a significant weight loss, indicating the toxicity of CDDP. Serum was isolated for the measurement of biochemical indexes of the kidney including BUN and CRE. The values obtained in combo free, free Pt−CUR and Pt−CUR@PSPPN treated groups stayed at a normal level, which was distinctly lower than that in CDDP treated group (Fig. 8B and C). One of the main factors of cisplatin toxicity was the induction of a high level of ROS in the kidney. Thus, we further detected and stained for biomarkers of ROS using red fluorescence. Fig. 8D shows that CDDP significantly increased the ROS level while the presence of CUR would reduce this

phenomenon, demonstrating the importance of the combination of these two drugs.

3.10. *In vivo anti-metastasis effect*

To determine the mechanism of the observed anti-tumor and anti-metastasis effects, A549 xenograft tumor sections mentioned above were stained with H&E and immunofluorescence after sacrifice for pathological evaluation (Fig. 9A). For H&E staining, the nuclei of tumors in mice treated with either PBS or free CUR showed active proliferation, displaying no significant apoptosis. In contrast, other groups exhibited varying degrees of necrosis and the most pyknosis and karyorrhexis were observed in nanoparticles treated mice. Immunofluorescence staining with CD31, VEGF, and MMP2 antibody was used to visualize the anti-metastasis effect of Pt−CUR *in vivo*. Cell nucleus was stained by DAPI with blue fluorescence and antibody signals were counterstained with red or green fluorescence, respectively. Significant reduction in metastasis markers was detected in the order of Pt−CUR@PSPPN > combo free > free Pt−CUR > free CUR > free CDDP, which was consistent with the results *in vitro*.

In order to further determine the *in vivo* anti-metastasis effect of Pt−CUR@PSPPN, bloodstream metastasis model was
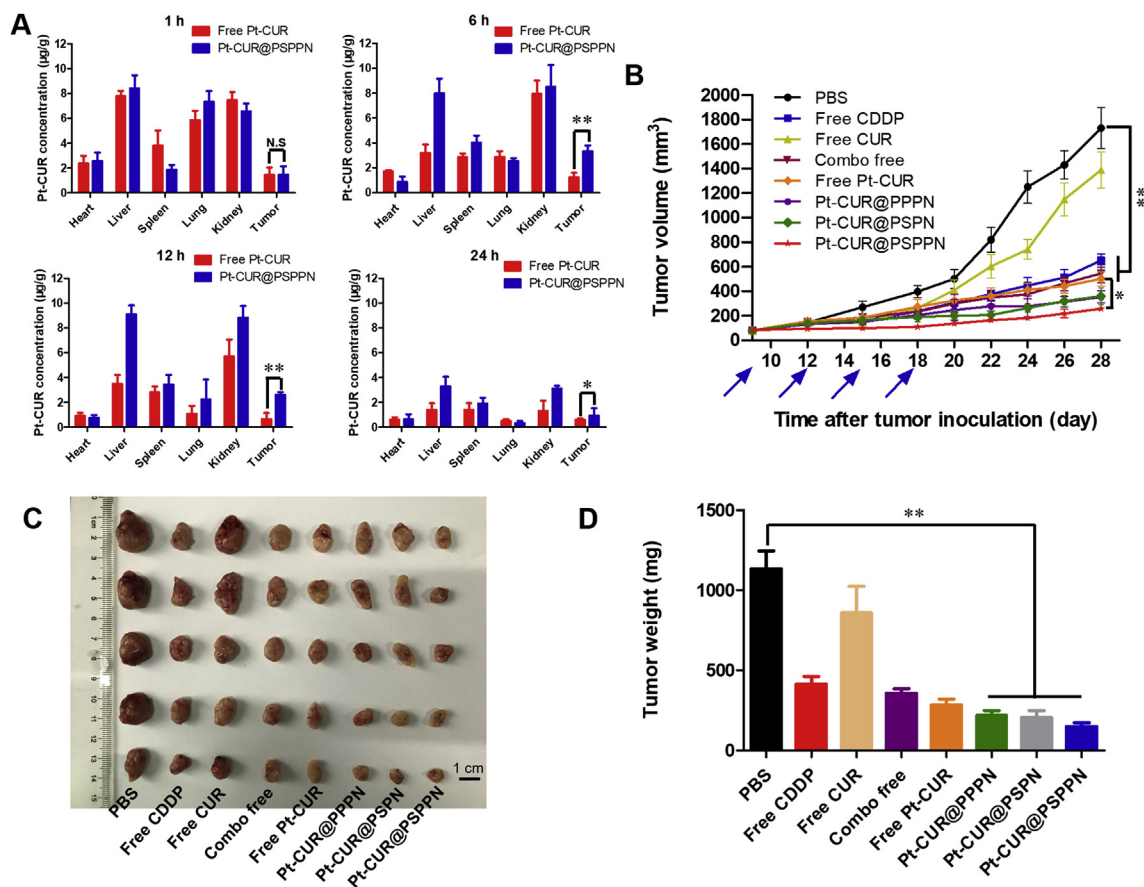
Figure 7 *In vivo* anti-tumor efficiency. (A) Biodistributions in A549 xenograft tumor-bearing nude mice tissues at 1, 6, 12 and 24 h after intravenous injection of free Pt−CUR and Pt−CUR@PSPPN. (B) Tumor growth curves during treatment. Mice were given tail vein injection of different drug formulations including free CDDP, free CUR, a combo of free drugs, free Pt−CUR as well as Pt−CUR@PPPN, Pt−CUR@PSPN, and Pt−CUR@PSPPN on day 9, 12, 15 and 18 after tumor inoculation. (C) Image and (D) weight of excised tumors at the end of the experiment (day 28 after tumor inoculation). Data are expressed as mean ± SD ($n = 5$). $^{*}P < 0.05$, $^{**}P < 0.01$.
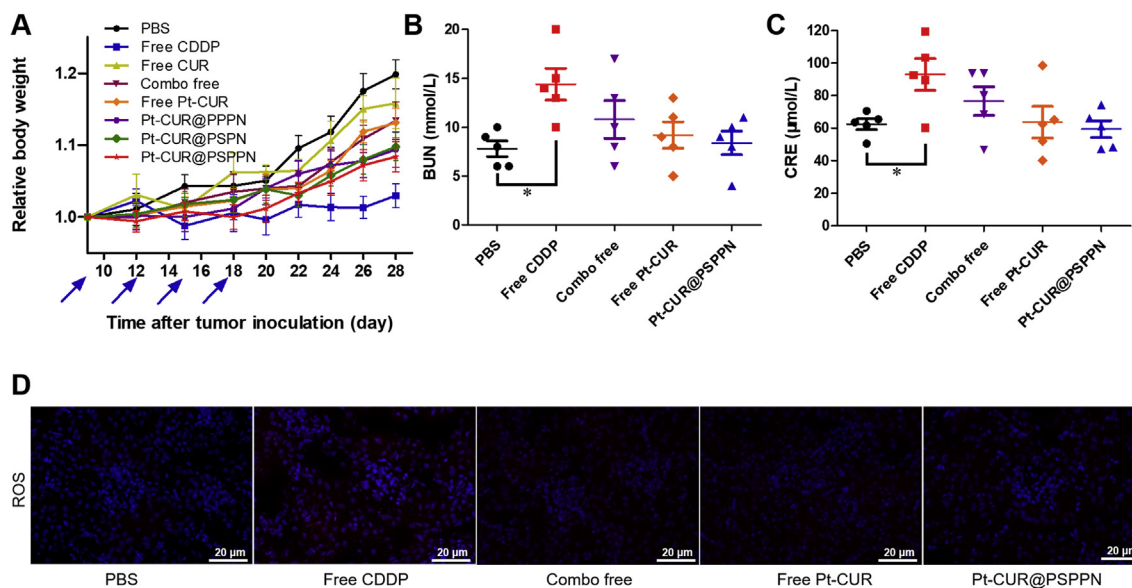
Figure 8 Results of systematic toxicity after treatment. (A) Relative body weight changes. The A549 xenograft tumor-bearing nude mice were injected four times with free CDDP, free CUR, combo of free drugs, free Pt−CUR, as well as Pt−CUR@PPPN, Pt−CUR@PSPN, and Pt−CUR@PSPPN. Values of biochemical indexes of kidney containing BUN (B) and CRE (C). (D) ROS levels in kidney. ROS was colored by red fluorescence and cell nucleus was counterstained by DAPI (blue fluorescence). Data are expressed as mean ± SD ($n = 5$). $^{*}P < 0.05$, $^{**}P < 0.01$.
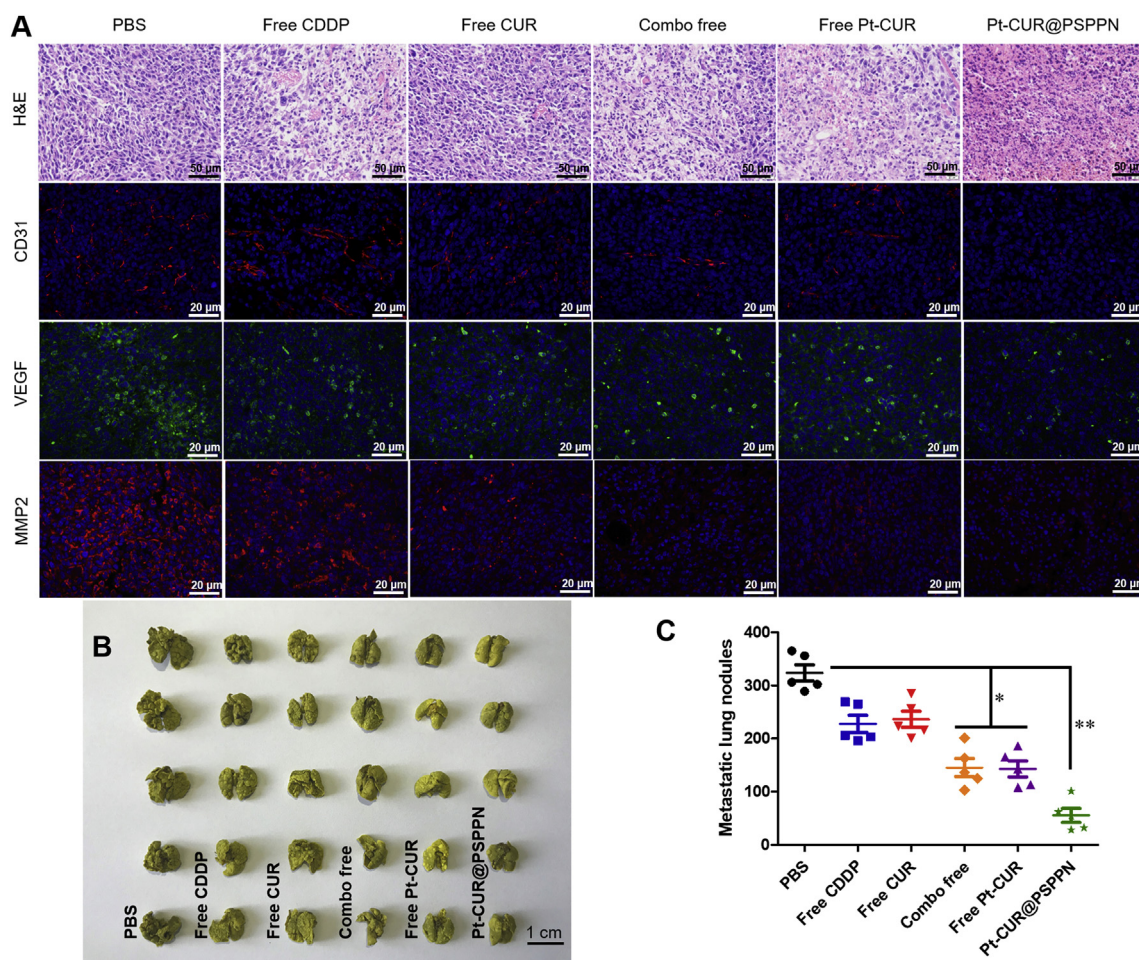
Figure 9 *In vivo* anti-metastasis effect. (A) H&E staining and immunohistochemical analysis including CD31, VEGF and MMP2 of A549 xenograft tumors. Cell nucleus was colored by DAPI with blue fluorescence and antibody signals were counterstained with red or green fluorescence. (B) Image of excised lungs in metastasis model at the end of the experiment. Mice were given tail vein injection of A549 cells and treated with PBS, free CDDP, free CUR, combo of free drugs, free Pt−CUR as well as Pt−CUR@PSPPN on day 2, 4, 6 and 8. (C) Quantitative analysis of the metastatic lung nodules. Data are expressed as mean ± SD ($n = 5$). *$P < 0.05$, **$P < 0.01$.

established. All drug formulations showed metastasis inhibition, which was observed from the image of excised lungs (Fig. 9B) and the count of metastatic lung nodules (Fig. 9C) at the end of the experiment. Although combination chemotherapy resulted in a greater inhibitory effect than single drug treatment, Pt−CUR@PSPPN presented much stronger metastasis inhibition than other drugs. The least metastatic nodules were found in the nanoparticle group.

4. Discussion

NSCLC is one of the most common malignancies and the leading cause of cancer death worldwide[1−5], most of which are associated with uncontrolled invasiveness and metastasis[41]. Chemotherapy, especially platinum-based chemotherapy plays an important role in the treatment of NSCLC[9−11]. CDDP, an effective agent, given alone or in combination with other chemotherapeutics drugs, has been widely used in the therapy of patients with NSCLC[42−44]. CDDP exerts anti-tumor effect mainly by forming cisplatin−DNA adduct, as well as by enhancing the ROS level[44]. However, these cytotoxic properties also result in the death of normal cells,

causing serious side effects[12,44]. Moreover, CDDP shows a litter inhibitory effect in lung cancer metastasis[45]. CUR is an acidic polyphenolic substance extracted from the rhizome of gingeraceae such as turmeric and has a remarkable antioxidant effect comparable to that of the potent antioxidant vitamin E[46]. In addition, markers of cancer metastasis including VEGF and MMP2 can be significantly down-regulated by the treatment of CUR[21,22]. Thus, combined chemotherapy of CDDP and CUR may reduce the side effects caused by enhanced ROS level, and show an increased anti-metastasis efficiency.

The problem of poor solubility severely limits the delivery of cisplatin[26]. In an early investigation, Wilson et al.[27] prepared a series of platinum complexes by activating CDDP and then reacting with different β-diketonate ligands. Their results indicated that CDDP modified by β-diketonate ligands predictably affected both the lipophilicity and reactivity of the resulting platinum complexes. Interestingly, CUR also contains a structure of β-diketonate. Therefore, we synthesized the platinum complexes of curcumin, Pt−CUR, which was a prodrug formulation for co-delivery CDDP and CUR.

To prove that the platinum compound could efficaciously dissociate from complexes to play its anti-tumor role,
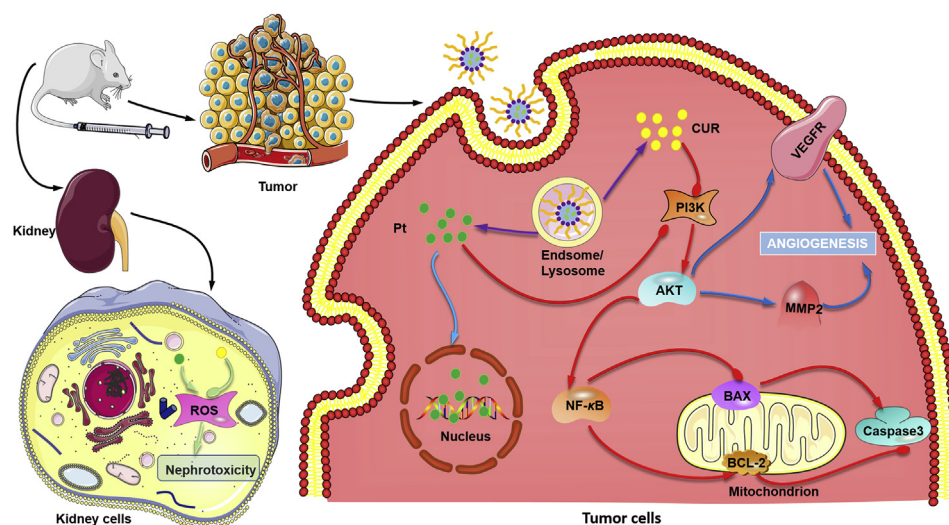
Figure 10 The overall mechanism of nanoparticles. Several mechanisms were believed to be responsible for reduced nephrotoxicity, synergistic anti-cancer effects, and enhanced anti-metastasis activity.

platinum−DNA adducts were examined by the usage of CP9/19 antibody[47]. Our study confirmed that Pt−CUR had a similar ability to bind to DNA as CDDP, which indicated the dissociable property. In the cytotoxicity and apoptosis studies including MTT assay, Hoechst 33258 staining, and Annexin V-APC/PI double staining study, both combination of free drugs and Pt−CUR showed an increased anti-cancer effect in A549 cells. In addition, combined therapy significantly suppressed migration and invasion of tumor cells. Compared with monotherapy, combination chemotherapy showed a better therapeutic effect both *in vitro* and *in vivo*. It has been reported that CUR can decrease the nephrotoxicity caused by CDDP, by reducing the level of ROS[48]. So the intracellular ROS level of HEK-293 cells was examined and CUR exhibited the potential to protect kidney cell treated with CDDP *in vitro*. *In vivo*, the related-biochemical indexes of the kidney (BUN and CRE) and ROS level were measured and showed negative results in Pt−CUR treated group. All these data collectively indicated that the combined formulation, Pt−CUR not only could reduce toxicity but also exert enhanced anti-cancer and anti-metastatic effects.

In this study, the significance of a drug carrier for delivery was also highlighted. Thus, we prepared pH and redox dual-responsive polymeric nanoparticles loaded with Pt−CUR (Pt−CUR@PSPPN). The nanoparticles were biocompatible and characterized with high drug loading capacity. The nanoparticles were able to release anti-tumor drugs in response to multiple stimulations, with the accelerated release of encapsulated drugs at the tumor microenvironment. Pt−CUR@PSPPN showed many advantages to deliver drugs, including enhanced cellular uptake and increased anti-cancer efficacy. In addition, Pt−CUR@PSPPN blocked PI3K/AKT signal transduction pathways and inhibited MMP2 and VEGFR2, resulting in enhanced anti-metastasis activity. The results of transwell and wound healing assays also illustrated this point. The particle size was about 100 nm, which had been reported to have excellent EPR effect, which should facilitate nanoparticle accumulation in tumor tissues. Biodistribution study in A549 xenograft tumor-bearing nude mice revealed that Pt−CUR@PSPPN increased the accumulation of drugs at the tumor site. Furthermore, nanoparticles significantly improved the anti-cancer effectiveness based on the synergistic effects and enhanced anti-metastasis activity, and reduced toxicity *in vivo*.

5. Conclusions

In summary, pH and redox dual-responsive nanoparticles loaded with Pt−CUR were developed. Several mechanisms might have contributed to reduced nephrotoxicity, synergistic anti-cancer effects, and enhanced anti-metastasis activity, as is summarized in Fig. 10. Therefore, Pt−CUR@PSPPN represents a promising approach to NSCLC.

Acknowledgments

Author contributions

Yan Chen, Xiang Ma, Tan Yang and Guangya Xiang conceived and designed the study. Yan Chen, Chen Chen, Xiaojuan Zhang and Chuanchuan He performed the *in vitro* experiments. Yan Chen, Pengxuan Zhao, Minsi Li, Ting Fan, Ruicong Yan performed the *in vivo* experiments. All authors analyzed the data and were involved in writing the manuscript.

Conflicts of interest

The authors have no conflicts of interest to declare.

Appendix A.   Supporting information

Supporting data to this article can be found online at https://doi.org/10.1016/j.apsb.2019.10.011.

References

1. Bray F, Ferlay J, Soerjomataram I, Siegel RL, Torre LA, Jemal A. Global cancer statistics 2018: GLOBOCAN estimates of incidence and mortality worldwide for 36 cancers in 185 countries. *CA Cancer J Clin* 2018;**68**:394−424.

2. Rotow J, Bivona TG. Understanding and targeting resistance mechanisms in NSCLC. *Nat Rev Cancer* 2017;**17**:637−58.

3. Hata A, Katakami N, Yoshioka H, Kaji R, Masago K, Fujita S, et al. Spatiotemporal T790M heterogeneity in individual patients with EGFR-mutant non-small-cell lung cancer after acquired resistance to EGFR-TKI. *J Thorac Oncol* 2015;**10**:1553−9.

4. Kumarakulasinghe NB, van Zanwijk N, Soo RA. Molecular targeted therapy in the treatment of advanced stage non-small cell lung cancer (NSCLC). *Respirology* 2015;**20**:370−8.

5. Wang T, Nelson RA, Bogardus A, Grannis Jr FW. Five-year lung cancer survival: which advanced stage nonsmall cell lung cancer patients attain long-term survival?. *Cancer* 2010;**116**:1518−25.

6. Chang A. Chemotherapy, chemoresistance and the changing treatment landscape for NSCLC. *Lung Cancer* 2011;**71**:3−10.

7. Kudinov AE, Deneka A, Nikonova AS, Beck TN, Ahn YH, Liu X, et al. Musashi-2 (MSI2) supports TGF-β signaling and inhibits claudins to promote non-small cell lung cancer (NSCLC) metastasis. *Proc Natl Acad Sci U S A* 2016;**113**:6955−60.

8. Shi L, Zhang B, Sun X, Lu S, Liu Z, Liu Y, et al. MiR-204 inhibits human NSCLC metastasis through suppression of NUAK1. *Br J Cancer* 2014;**111**:2316−27.

9. Garon EB, Rizvi NA, Hui R, Leighl N, Balmanoukian AS, Eder JP, et al. Pembrolizumab for the treatment of non-small-cell lung cancer. *N Engl J Med* 2015;**372**:2018−28.

10. Arriagada R, Bergman B, Dunant A, Le Chevalier T, Pignon JP, Vansteenkiste J. Cisplatin-based adjuvant chemotherapy in patients with completely resected non-small-cell lung cancer. *N Engl J Med* 2004;**350**:351−60.

11. Wang D, Lippard SJ. Cellular processing of platinum anticancer drugs. *Nat Rev Drug Discov* 2005;**4**:307−20.

12. Yao X, Panichpisal K, Kurtzman N, Nugent K. Cisplatin nephrotoxicity: a review. *Am J Med Sci* 2007;**334**:115−24.

13. Yang T, Chen Y, Zhao P, Xue H, You J, Li B, et al. Enhancing the therapeutic effect *via* elimination of hepatocellular carcinoma stem cells using Bmi1 siRNA delivered by cationic cisplatin nanocapsules. *Nanomedicine* 2018;**14**:2009−21.

14. Jovanovic SV, Steenken S, Boone CW, Simic MG. H-atom transfer is a preferred antioxidant mechanism of curcumin. *J Am Chem Soc* 1999;**121**:9677−81.

15. Rahmani S, Asgary S, Askari G, Keshvari M, Hatamipour M, Feizi A, et al. Treatment of non-alcoholic fatty liver disease with curcumin: a randomized placebo-controlled trial. *Phytother Res* 2016;**30**:1540−8.

16. Yousef MI, Omar SA, El-Guendi MI, Abdelmegid LA. Potential protective effects of quercetin and curcumin on paracetamol-induced histological changes, oxidative stress, impaired liver and kidney functions and haematotoxicity in rat. *Food Chem Toxicol* 2010;**48**:3246−61.

17. Wang J, Wang H, Zhu R, Liu Q, Fei J, Wang S. Anti-inflammatory activity of curcumin-loaded solid lipid nanoparticles in IL-1β transgenic mice subjected to the lipopolysaccharide-induced sepsis. *Biomaterials* 2015;**53**:475−83.

18. Qin Y, Lin L, Chen Y, Wu S, Si X, Wu H, et al. Curcumin inhibits the replication of enterovirus 71 *in vitro*. *Acta Pharm Sin B* 2014;**4**:284−94.

19. Yallapu MM, Khan S, Maher DM, Ebeling MC, Sundram V, Chauhan N, et al. Anti-cancer activity of curcumin loaded nanoparticles in prostate cancer. *Biomaterials* 2014;**35**:8635−48.

20. Kuhad A, Pilkhwal S, Sharma S, Tirkey N, Chopra K. Effect of curcumin on inflammation and oxidative stress in cisplatin-induced experimental nephrotoxicity. *J Agric Food Chem* 2007;**55**:10150−5.

21. Kunnumakkara AB, Anand P, Aggarwal BB. Curcumin inhibits proliferation, invasion, angiogenesis and metastasis of different cancers through interaction with multiple cell signaling proteins. *Cancer Lett* 2008;**269**:199−225.

22. Lin SS, Lai KC, Hsu SC, Yang JS, Kuo CL, Lin JP, et al. Curcumin inhibits the migration and invasion of human A549 lung cancer cells through the inhibition of matrix metalloproteinase-2 and-9 and vascular endothelial growth factor (VEGF). *Cancer Lett* 2009;**285**:127−33.

23. Brigger I, Dubernet C, Couvreur P. Nanoparticles in cancer therapy and diagnosis. *Adv Drug Deliv Rev* 2002;**54**:631−51.

24. Chen Y, Cheng Y, Zhao P, Zhang S, Li M, He C, et al. Co-delivery of doxorubicin and imatinib by pH sensitive cleavable PEGylated nanoliposomes with folate-mediated targeting to overcome multidrug resistance. *Int J Pharm* 2018;**542**:266−79.

25. Acharya S, Sahoo SK. PLGA nanoparticles containing various anticancer agents and tumour delivery by EPR effect. *Adv Drug Deliv Rev* 2011;**63**:170−83.

26. Guo S, Wang Y, Miao L, Xu Z, Lin CM, Zhang Y, et al. Lipid-coated cisplatin nanoparticles induce neighboring effect and exhibit enhanced anticancer efficacy. *ACS Nano* 2013;**7**:9896−904.

27. Wilson JJ, Lippard SJ. *In vitro* anticancer activity of cis-diammineplatinum(II) complexes with β-diketonate leaving group ligands. *J Med Chem* 2012;**55**:5326−36.

28. Zhang T, Chen Y, Ge Y, Hu Y, Li M, Jin Y. Inhalation treatment of primary lung cancer using liposomal curcumin dry powder inhalers. *Acta Pharm Sin B* 2018;**8**:440−8.

29. Zhang F, Ni Q, Jacobson O, Cheng S, Liao A, Wang Z, et al. Polymeric nanoparticles with a glutathione-sensitive heterodimeric multifunctional prodrug for *in vivo* drug monitoring and synergistic cancer therapy. *Angew Chem Int Ed Engl* 2018;**57**:7066−70.

30. Ganta S, Devalapally H, Shahiwala A, Amiji M. A review of stimuli-responsive nanocarriers for drug and gene delivery. *J Control Release* 2008;**126**:187−204.

31. Wang X, Dai J, Chen Z, Zhang T, Xia G, Nagai T, et al. Bioavailability and pharmacokinetics of cyclosporine A-loaded pH-sensitive nanoparticles for oral administration. *J Control Release* 2004;**97**:421−9.

32. Yang S, Tang Z, Zhang D, Deng M, Chen X. pH and redox dual-sensitive polysaccharide nanoparticles for the efficient delivery of doxorubicin. *Biomater Sci* 2017;**5**:2169−78.

33. Chen G, Wang Y, Xie R, Gong S. Tumor-targeted pH/redox dual-sensitive unimolecular nanoparticles for efficient siRNA delivery. *J Control Release* 2017;**259**:105−14.

34. Cheng J, Teply BA, Sherifi I, Sung J, Luther G, Gu F, et al. Formulation of functionalized PLGA-PEG nanoparticles for *in vivo* targeted drug delivery. *Biomaterials* 2007;**28**:869−76.

35. Mitra K, Gautam S, Kondaiah P, Chakravarty AR. The cis-diammineplatinum(II) complex of curcumin: a dual action DNA cross-linking and photochemotherapeutic agent. *Angew Chem Int Ed Engl* 2015;**54**:13989−93.

36. Liu C, Yuan J, Luo X, Chen M, Chen Z, Zhao Y, et al. Folate-decorated and reduction-sensitive micelles assembled from amphiphilic polymer−camptothecin conjugates for intracellular drug delivery. *Mol Pharm* 2014;**11**:4258−69.

37. Chou TC, Talalay P. Quantitative analysis of dose-effect relationships: the combined effects of multiple drugs or enzyme inhibitors. *Adv Enzyme Regul* 1984;**22**:27−55.

38. Owen SC, Chan DPY, Shoichet MS. Polymeric micelle stability. *Nano Today* 2012;**7**:53−65.

39. Missirlis D, Kawamura R, Tirelli N, Hubbell JA. Doxorubicin encapsulation and diffusional release from stable, polymeric, hydrogel nanoparticles. *Eur J Pharm Sci* 2006;**29**:120−9.

40. Raza MK, Mitra K, Shettar A, Basu U, Kondaiah P, Chakravarty AR. Photoactive platinum(ii) β-diketonates as dual action anticancer agents. *Dalton Trans* 2016;**45**:13234−43.

41. Temel JS, Greer JA, Muzikansky A, Gallagher ER, Admane S, Jackson VA, et al. Early palliative care for patients with metastatic non-small-cell lung cancer. *N Engl J Med* 2010;**363**:733−42.

42. Zhong WZ, Wang Q, Mao WM, Xu ST, Wu L, Shen Y, et al. Gefitinib *versus* vinorelbine plus cisplatin as adjuvant treatment for stage II−IIIA (N1−N2) EGFR-mutant NSCLC (ADJUVANT/CTONG1104): a randomised, open-label, phase 3 study. *Lancet Oncol* 2018;**19**:139−48.

43. Gatzemeier U, Pluzanska A, Szczesna A, Kaukel E, Roubec J, De Rosa F, et al. Phase III study of erlotinib in combination with cisplatin and gemcitabine in advanced non-small-cell lung cancer: the tarceva lung cancer investigation trial. *J Clin Oncol* 2007;**25**:1545−52.

44. Dasari S, Tchounwou PB. Cisplatin in cancer therapy: molecular mechanisms of action. *Eur J Pharmacol* 2014;**740**:364−78.

45. Yu H, Guo C, Feng B, Liu J, Chen X, Wang D, et al. Triple-layered pH-responsive micelleplexes loaded with siRNA and cisplatin prodrug for NF-kappa B targeted treatment of metastatic breast cancer. *Theranostics* 2016;**6**:14−27.

46. Rezaee R, Momtazi AA, Monemi A, Sahebkar A. Curcumin: a potentially powerful tool to reverse cisplatin-induced toxicity. *Pharmacol Res* 2017;**117**:218−27.

47. Miao L, Guo S, Zhang J, Kim WY, Huang L. Nanoparticles with precise ratiometric co-loading and co-delivery of gemcitabine monophosphate and cisplatin for treatment of bladder cancer. *Adv Funct Mater* 2014;**24**:6601−11.

48. Waseem M, Kaushik P, Parvez S. Mitochondria-mediated mitigatory role of curcumin in cisplatin-induced nephrotoxicity. *Cell Biochem Funct* 2013;**31**:678−84.